Bull. Mater. Sci., Vol. 39, No. 1, February 2016, pp. 125–131. © Indian Academy of Sciences.

Effect of Bi and Sr doping on morphological and magnetic properties of $LaCo_{0.6}Fe_{0.4}O_3$ nanosized perovskites

U MEGHA[1,*], GEORGE VARGHESE[2] and K SHIJINA[1]

[1]Department of Physics, University of Calicut, Kerala 673635, India

[2]Kerala State Council for Science, Technology and Environment, Thiruvananthapuram, Kerala 695004, India

MS received 9 July 2015; accepted 19 October 2015

Abstract. Nanopowders of $La_{1-x}Bi_xCo_{0.6}Fe_{0.4}O_3$ ($x = 0$, 0.1, 0.2) and $La_{1-2x}Bi_xSr_xCo_{0.6}Fe_{0.4}O_3$ ($x = 0.1$) multinary perovskites were synthesized by citrate sol–gel autocombustion method. Crystalline phase and the lattice parameters were obtained from X-ray diffraction pattern. The XRD result shows that all compounds have rhombhohedral crystal structure with $R\bar{3}c$ space group and Bi ($x = 0.2$) have the presence of secondary peaks. Crystallite size, dislocation density, specific area and strain were calculated from XRD. The elemental composition and micrographs of grain were obtained from EDAX (energy dispersive X-ray analysis) and SEM (scanning electron microscopy), with an average grain size below 400 nm. Surface morphological studies using XPS (X-ray photoelectron spectroscopy) were used to find out the chemical states and surface proportion of oxygen present in samples. Finally, using the vibrating sample magnetometer the room temperature magnetic behaviour of compounds was studied and it was observed that the ferromagnetic behaviour of $LaCo_{0.6}Fe_{0.4}O_3$ was reduced by Bi and Sr doping.

Keywords. Perovskites; nanosized; citrate sol–gel autocombustion method; Williamson's Hall plot; X-ray photoelectron spectroscopy; vibrating sample magnetometer.

1. Introduction

Investigating spin magnetic properties of perovskites is an interesting research as the ABO_3-type metal oxides, especially rare earth perovskites, exhibit unusual magneto-transport properties. The lanthanum-based perovskites have displayed strong magneto-transport properties even by simple alteration of its chemical composition. Ranging from insulating phase to conducting, antiferromagnetic to ferromagnetic, low magnetostriction to gaint magnetoresistance, its properties change by inducing stoichiometric changes in composition. Ionic size effect or ionic valence effect in doped perovskites ($A_{1-x}\cdot A'_x\cdot BO_3$ or $AB_{1-y}\cdot B'_y\cdot O_3$) results in the magneto-transport properties in these compounds. Change in unit cell volume due to substitution favours spin transitions in $LaCoO_3$ perovskites [1,2]. The complex spin structure of Co ions in perovskite gives us plenty of opportunities to explore the exotic magnetic phenomenon of these materials. The Co ions in $LaCoO_3$ can exist in three different spin states; low spin LS ($t_{2g}^6\ e_g^0$ for Co^{3+} and $t_{2g}^5\ e_g^0$ for Co^{4+}), intermediate spin IS ($t_{2g}^5\ e_g^1$ for Co^{3+} and $t_{2g}^4\ e_g^1$ for Co^{4+}) and high spin state HS ($t_{2g}^4\ e_g^2$ for Co^{3+} and $t_{2g}^3\ e_g^2$ for Co^{4+}), which can induce spin entropic effect to the perovskite structure and can influence all the magneto-transport properties of the materials [3]. The existence of three spin states in Co makes it a potential candidate for magnetic applications. The LS state of $LaCoO_3$ is nonmagnetic, while at temperature above 100 K it undergoes transition to magnetic state, which is either IS or HS state [4]. It was reported by Rodriguez and Goodenough [5] that, the reason for ferromagnetism in these compounds is due to the double exchange or by super exchange mechanism between Co^{3+} and Co^{4+}. The magnetic interaction between Co^{3+} ions and Co^{4+} ions is responsible for spin–glass transitions and the properties may considerably change if chemical in homogeneities are created in the system. Substituting La^{3+} ions by alkaline earth metals will produce huge anisotropic magnetostriction and ferromagnetic ordering with Curie temperature below 250 K. This has been investigated extensively in $La_{1-x}Sr_xCoO_3$ system by many researches, focusing into the three spin states of cobalt ions. The Zener double exchange mechanism gives a reasonable explanation for the process that is involved in magnetic transitions [6]. The Sr^{2+} ions when replacing La^{3+} sites in $La_{1-x}Sr_xCoO_3$ produce holes, which may reside at either low spin ($t_{2g}^5\ e_g^0$) or intermediate spin ($t_{2g}^5\ e_g^1$) state of Co^{4+} ions. The neighbouring Co^{3+} and Co^{4+} will engage in ferromagnetic double exchange interaction with oxygen. It has been further noticed that the doped holes will create nanosized clusters which upon increasing Sr concentration will grow in size and multiply in number. These clusters in fact trigger antiferromagnetic superexchange between Co^{3+} ions, which normally lie at the boundaries. Ferromagnetic as well as antiferromagnetic exchange interaction results in spin glass behaviour even below the magnetic ordering temperature [7].

Instead of substituting A-sites, substitution of B-site i.e., Co ions by Fe^{3+} ($3d^5$), Mn^{4+}($3d^3$) or Ni^{3+}($3d^7$) has found

*Author for correspondence (meghaunikoth@gmail.com)

to reverse the effects of Sr^{2+} doping at La^{3+} sites. Most of the works found in literature focuses on the studies of A-site doping, whereas the influence of B-site doping on magnetoelectric properties still remain unexplored. Fe^{3+} and Ni^{3+} doping at B-site were mostly preferred because Fe^{3+} has one spin less and Ni^{3+} has one spin more than that of Co^{3+} ion. The influences of both Fe and Ni ($LaCo_{1-x}B_xO_3$; B = Fe, Ni) had been investigated by Yu *et al*. Ni^{3+} doping makes it ferromagnetic at lighter level of doping (above 10%) and at $x < 0.5$, sample exhibits spin glass behaviour at low temperatures and negative giant magnetoresistance. Troyanchuk *et al* studied the magnetic properties of Fe-doped $LaCoO_3$, and they reported that with low Fe content it has paramagnetic or antiferromagnetic state. In about 10% of Fe, it experiences gradual transition to diamagnetic state even at temperature around 100 K. For $x \geq 0.4$ it has small spontaneous magnetic moment and at $T_N = 120$ K, it becomes fully paramagnetic which is not a characteristic of spin glass. The Fe doping in fact stabilizes the Co ions to a low spin state. They also found that unit cell parameters of $LaCo_{1-x}Fe_xO_3$ crystallites grow more or less linearly with Fe addition favouring low spin states of Co ions in it. Reduction of samples with $x = 0.5$ promotes oxygen vacancies and increases magnetic anisotropy. Near the oxygen vacancies Co^{2+} or Co^{3+} in HS states is produced causing single ion magnetic anisotropy. Fe incorporation weakens Co–O bond in the CoO_6 octahedra. However, it is observed that majority of Co^{3+} ions prefer to remain in LS state as in $LaCoO_3$. Modelling of the magnetic properties of $LaCo_{1-x}Fe_xO_3$ system defines Co^{3+} ions in LS state, with less exchange interactions. Weak ferromagnetism and large magnetic anisotropy are attributed to the Fe^{3+} ions in the system [8,9].

These materials have a lot of other applications as sensors, catalysts and electrodes in solid oxide fuel cells, thermoelectric devices etc. Vulchev *et al* [10] studied the thermoelectric property of Fe- and Ni-doped $LaCoO_3$. They reported that at room temperature $LaCo_{1-x}Fe_xO_3$ ($x = 0.05$) has a figure of merit ZT = 0.04, above than that of $LaCoO_3$ (ZT < 0.01) and double substitution of both yields better thermoelectric efficiency with ZT = 0.16 [10]. Bin *et al* [11] reported that $LaCo_{1-x}Fe_xO_3$ can be used as catalysts for the simultaneous removal of NO_x carbon soot and the performances decreases with the increase in Fe content. From dielectric studies Ge *et al* [12] have concluded that these compounds show p-type semiconducting properties as well as high sensitivity towards ethanol sensing. Royer *et al* [13] tested the catalytic activity of these compounds for methane oxidation and its resistance to SO_2 poisoning using nanopowders of these compounds.

In this experimental study, we have synthesized nanopowders of title compounds by citrate sol–gel autocombustion method, in which polyesterification of ethylene glycol and citric acid leads to the formation of metal–polymer complex [14]. The influence on substitution of La-site by bismuth and strontium in $LaCo_{0.6}Fe_{0.4}O_3$ was investigated, which was not studied so far. Bi has the presence of a lone pair, which arises as the result of hybridization of $6s$ and $6p$ atomic orbitals with $6s^2$ electrons that can modify the properties of ferroelectric, magnetic and thermoelectric materials [15]. Meanwhile Sr substitution does not change the crystal structure of perovskites, but creates oxygen vacancy which leads to the enhancement of conductivity [16].

2. Experimental

The double-substituted perovskites $LaCo_{0.6}Fe_{0.4}O_3$ (L0), $La_{0.9}Bi_{0.1}Co_{0.6}Fe_{0.4}O_3$ (L1), $La_{0.8}Bi_{0.2}Co_{0.6}Fe_{0.4}O_3$ (L2) and $La_{0.8}Bi_{0.1}Sr_{0.1}Co_{0.6}Fe_{0.4}O_3$ (L3) were prepared by polymerizable complex method. Stoichiometric amounts of $La(NO_3)_3{\cdot}6H_2O$, $Co(NO_3)_2{\cdot}6H_2O$, $Fe(NO_3)_3{\cdot}9H_2O$, $Bi(NO_3)_3{\cdot}9H_2O$, $Sr(NO_3)_2$, citric acid and ethylene glycol were accurately weighed (all from Sigma Aldrich, 99.99–99% purity) and dissolved in conc. nitric acid and deionized water. The solution was stirred and heated to form polymer complex, which had undergone decomposition followed by autocombustion to form fine heap of powders. The calcined powders at 700°C for 6 h were ground well using agate mortar, pressed into cylindrical pellets and sintered at 900°C for 8 h.

The crystalline phases and the lattice constants of compounds were determined using Rigaku Miniflex 600 X-ray diffractometer in the range 20–80° with CuKα radiation at room temperature. Scanning electron microscope (Carl Zeiss Ultra 55 FE-SEM) equipped with an energy dispersive X-ray analysis unit was used for studying the elemental composition and morphology of the powders. X-ray photoelectron core-level spectra were measured for bulk samples using Axis Ultra DLD Kratos with MgKα source with excitation of energy 1253.68 eV. Room temperature magnetic hysteresis (M–H) loop was obtained using (Lake Shore: Model: 7404) vibrating sample magnetometer.

3. Results and discussions

The diffraction peaks of the single- and double-substituted perovskites (L0, L1, L2, L3) and the variation of lattice constants with various doping concentrations of Bi and Sr are shown in figure 1. The patterns fit in the frame work of a rhombhohedral $LaCoO_3$ type structure ($a = b \neq c$ and $\alpha = \beta = 90°$, $\gamma = 120°$) with $R\bar{3}c$ space group (ICDD: 00-053-1211). Only one compound (L2) for which the Bi substitution is $x = 0.2$ shows the presence of a secondary peak. The changes in lattice parameters reflect the influence of metal ion substitution in the samples. The lattice parameters were obtained using PDXL software and are tabulated in table 1. Debye–Scherrer formula was used for calculating the crystallite size. For Bi ($x = 0.1$) and Sr ($x = 0, 0.1$) the lattice constant increases obeying Vigard's law [17] with Bi ($x = 0.2$), it exceeds the solubility limit and hence shows the presence of secondary peak as well as decrease in lattice constant. Tolerance factor was calculated using Goldschmidt formula [18].

Dislocation is a crystallographic defect that has prominent role in influencing the physical properties of materials. The hardness of material varies with dislocation density and

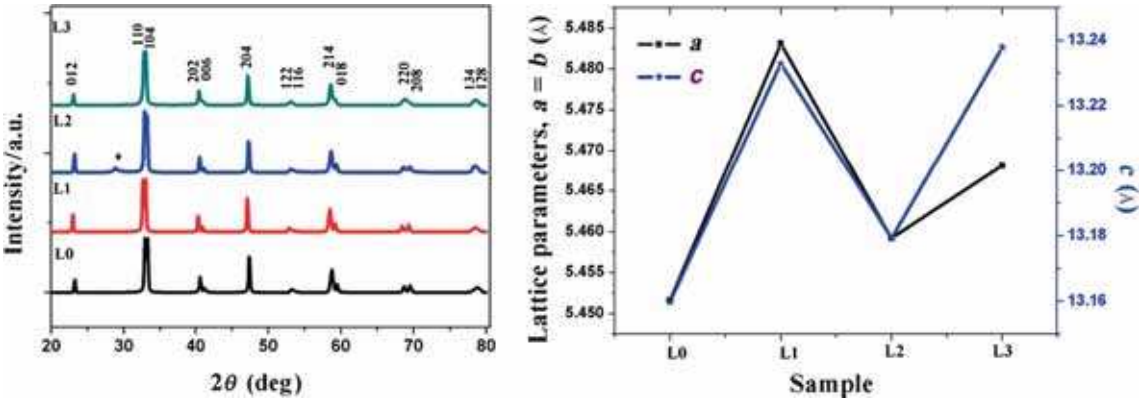

Figure 1. XRD patterns of samples L0, L1, L2 and L3, and variation of lattice parameters with doping.

Table 1. Lattice parameters, volume and tolerance factor of single-and double-doped $LaCo_{0.6}Fe_{0.4}O_3$.

Samples	Lattice parameters $a = b$ (Å)	Lattice parameter c (Å)	Unit cell volume (Å)^3	Tolerance factor
$LaCo_{0.6}Fe_{0.4}O_3$(L0)	5.4516	13.1590	268.6203	0.989
$La_{0.9}Bi_{0.1}Co_{0.6}Fe_{0.4}O_3$ (L1)	5.4831	13.2320	268.6203	0.977
$La_{0.8}Bi_{0.2}Co_{0.6}Fe_{0.4}O_3$ (L2)	5.4592	13.1793	268.6217	0.965
$La_{0.8}Bi_{0.1}Sr_{0.1}Co_{0.6}Fe_{0.4}O_3$ (L3)	5.4681	13.2370	268.6203	0.979

Table 2. Crystallite size, dislocation density, specific surface area from XRD data and strain from W–H plot for L0, L1, L2 and L3.

	Dislocation density ($\times 10^{15}$ m^{-2})				
Crystallite size (nm)	(012)	(110)	(202)	Specific surface area (m^2 g^{-1})	Strain
37.1	0.7447	0.7287	0.7115	22.50	0.0014
44.7	0.5060	0.4959	0.4804	19.00	0.0013
37.3	0.7347	0.7211	0.7037	22.48	0.0015
36.4	0.7793	0.7629	0.7423	23.21	0.0016

grain size. The strong interplay between inter-granular and intra-granular deformation processes in the hardness of microstructures were well discussed up to a certain limit (∼20 nm) and it was reported that grain size and hardness are inversely varying factors. The dislocation densities (δ) as well as specific surface area are determined from XRD data, using the equations:

$$\delta = 15\beta \cos\theta/4aD, \tag{1}$$

$$S = 6 \times 10^3/D\rho, \tag{2}$$

where β is full-width at half maximum (in radians), θ the Bragg's diffraction angle (in degree), a lattice constant (in nm), D the particle size (in nm) and ρ the density of samples (in g m^{-3}). For a small crystallite size the specific surface area will be large. Williamson's Hall plot $\beta \cos\theta$ *vs*. $\sin\theta$ was used for calculating the strain value and are tabulated in table 2 [19]. Dislocations are by and large in different crystal planes. A marginal reduction in specific surface area, strain as well as dislocation density is observed for 44.7 nm size crystallites.

Dense nanostructures with well-shaped grain boundaries were seen in SEM micrographs with average grain size ranging from 200 to 400 nm (figure 2). EDAX confirms the

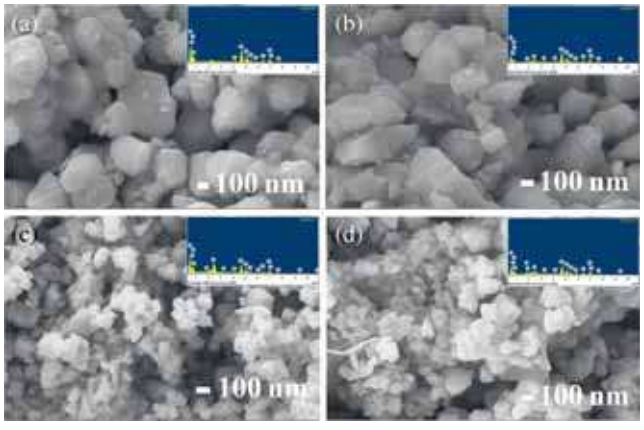

Figure 2. SEM micrographs and EDAX spectrum of (**a**) L0 (**b**) L1 (**c**) L2 and (**d**) L3.

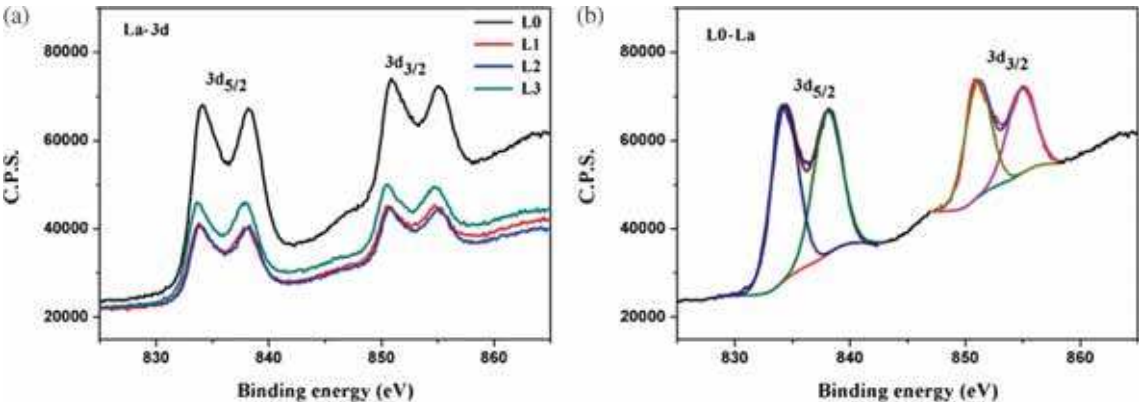

Figure 3. XPS spectra of (**a**) La-3d in L0, L1, L2 and L3, (**b**) peak fitting of La in L0.

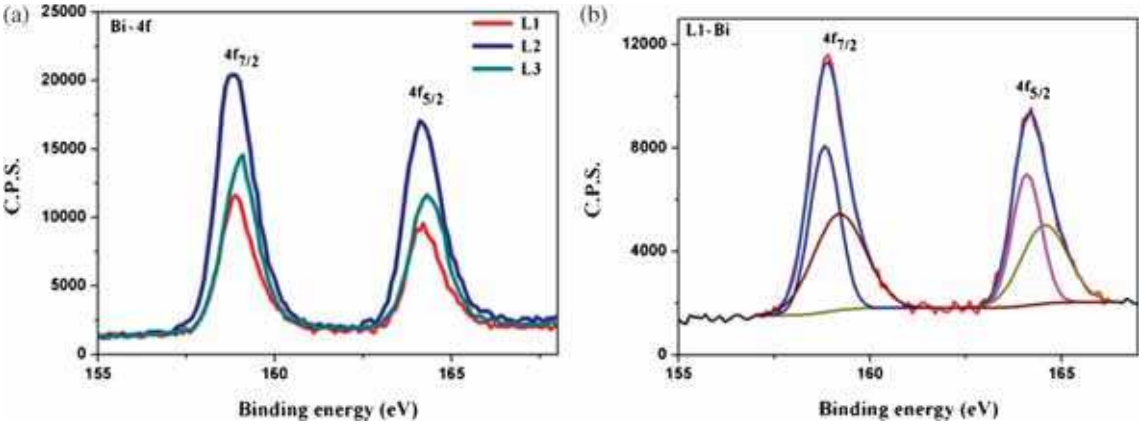

Figure 4. XPS spectra of (**a**) Bi-4f in L1, L2 and L3, (**b**) peak fitting of Bi in L1.

Table 3. XPS peak positions (binding energy, eV) of elements.

	Binding energies (eV)			
Samples	L0	L1	L2	L3
La-$3d_{3/2}$	854.8	854.5	854.7	854.4
	851.1	850.7	850.9	850.6
La-$3d_{5/2}$	838	837.7	837.9	837.6
	834.3	833.9	834.1	833.8
Bi-$4f_{5/2}$	—	164.5	164.6	164.4
	—	164.1	164.1	164.3
Bi-$4f_{7/2}$	—	159.2	159	159.1
	—	158.8	158.7	158.9
Sr-$3d_{3/2}$	—	—	—	134.2
Sr-$3d_{5/2}$	—	—	—	132.4
Co-$2p_{1/2}$	795.6	795.4	795.3	795.5
Co-$2p_{3/2}$	780.4	780.2	780.2	780.3
Co-satellite	790.5	789.9	790.4	789.7
Fe-$2p_{1/2}$	724.1	723.9	723.8	724
Fe-$2p_{3/2}$	710.7	710.6	710.6	710.5
Fe-satellite	714.4	714.6	714.5	714.8
O-1s	531.6	531.6	531.2	531.3
	529.4	529.3	529.4	529.2
O_A/O_L	1.09	0.93	0.81	1.22

elemental composition of compounds. The pictures show that the heavily doping changes shape remarkably. The particle size has been decreased with the Bi and Sr (L2 and L3) and become highly agglomerated. However for L0 and L1 the particle morphology is well defined.

The XPS spectra obtained for the core-level peaks of constituent elements of the compounds are analysed by PEAKFIT41 software with a Shirley background subtraction and Lorentizian/Gaussian peak shape [20–22]. Carbon 1s peak was considered at 285 eV and error in binding energy is 0.1 eV [23].

The narrow scan of core-level X-ray photoelectron spectra (XPS) of lanthanum in compounds L0, L1, L2 and L3 are shown in figure 3a, while panel b shows the peak fitted La *3d* spectrum consisting of doublet line with *3/2* and *5/2* spins due to the interaction between the spins of the electron and its

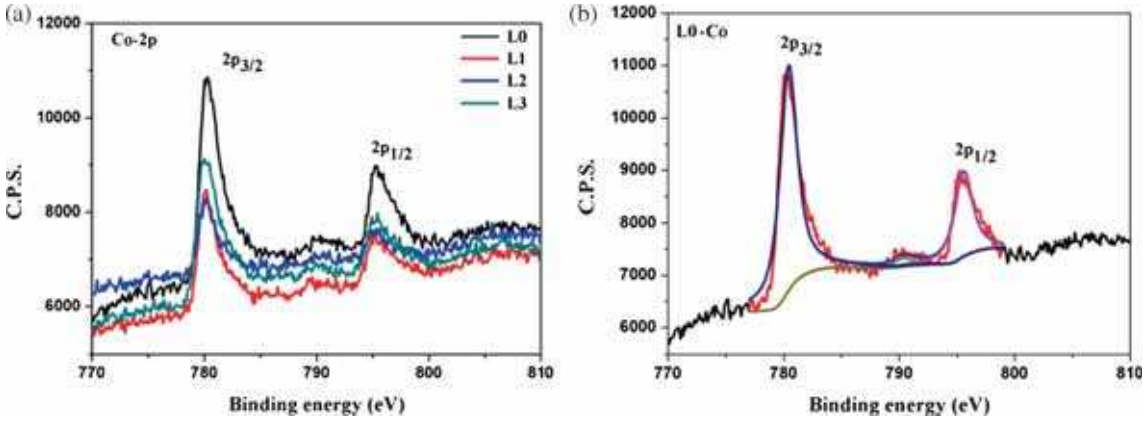

Figure 5. XPS spectra of (**a**) Co-2p in L0, L1, L2 and L3, (**b**) peak fitting of Co in L0.

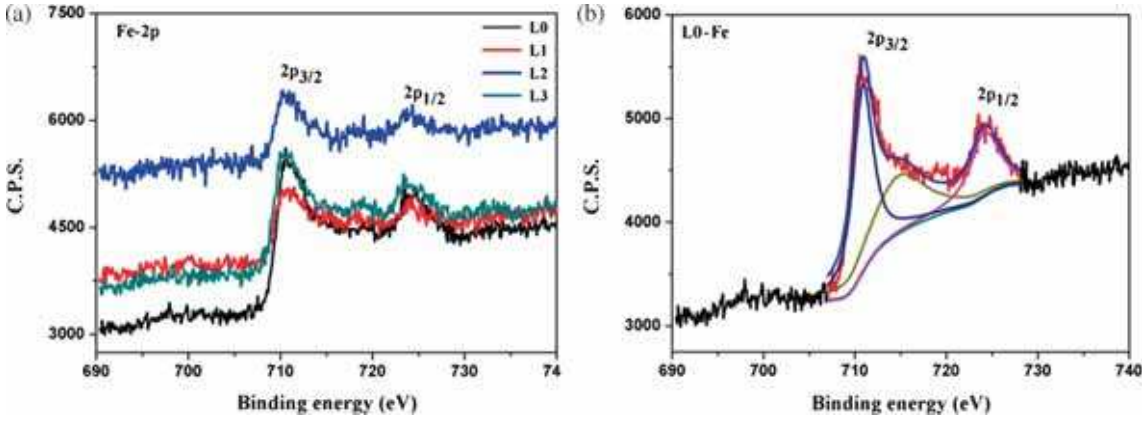

Figure 6. XPS spectra of (**a**) Fe-2p in L0, L1, L2 and L3, (**b**) peak fitting of Fe in L0.

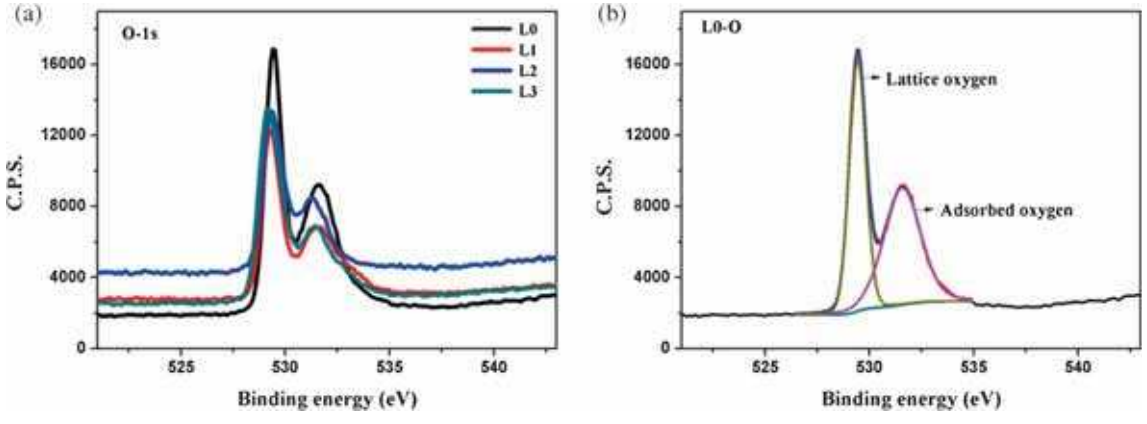

Figure 7. (**a**) O-1s in L0, L1, L2 and L3, (**b**) peak fitting of O-1s in L0.

orbital angular momentum. This interaction leads to a splitting of the degenerate state into two components. Slight shift in binding energies was noticed due to the Bi doping. The binding energy value suggests that all compounds have similar perovskite structure. The peaks due to Bi (4f) are shown in figure 4a, while panel b shows doublet components with *5/2* and *7/2* spins [24]. Binding energy values of all elements are tabulated in table 3. The sharp La 3d and Bi *4f* peak shows that the La and Bi have valency +3 without valence instability.

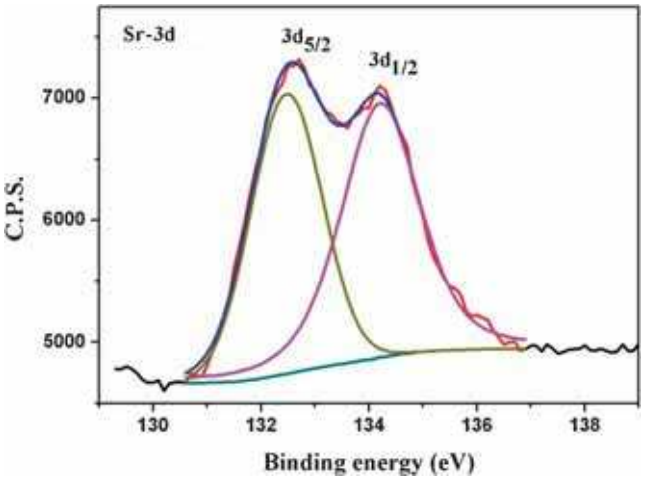

Figure 8. XPS spectra of Sr-3d in L3.

The core-level energy spectrum shown in figures 5 and 6 of cobalt and iron arises from the *2p* shell which normally constitute doublets such as Co $2p_{1/2}$ and Co $2p_{3/2}$ at regions 795.4 and 780.5 eV (Co^{3+}), with a binding energy splitting of ∼15.2 eV which is in good agreement with the previous literature data. For iron, $2p_{1/2}$ and $2p_{3/2}$ at regions are at 724 and 710.5 eV (Fe^{3+}), respectively, with satellite peaks. The presence of satellite peaks in Co and Fe spectra may be due to the presence of Co^{2+} and Fe^{2+}. The O-1s, as shown in figure 7, has the presence of two peaks: one at 528.7–530.4 eV gives the lattice oxygen (O_L) which indicates the metal oxygen bond and other at 531.6–531.8 eV corresponds to the regular adsorbed oxygen (O_A), such as O^-, O^{2-} and O_2^{2-} [25]. The ratio of adsorbed oxygen to lattice oxygen has importance when we consider the catalytic performance of perovskite oxides. This value determines the number of oxygen vacancies created during doping. The ratio was calculated and is tabulated in table 3. The sharp Sr-3d peak in figure 8 suggests the presence of Sr^{2+} oxidation state [26].

The variation of magnetic moment with field for Bi- and Sr-doped $LaCo_{0.6}Fe_{0.4}O_3$ is shown in figure 9. The parent compound L0 has the presence of small spontaneous magnetic moment and is a weak ferromagnet with coercivity

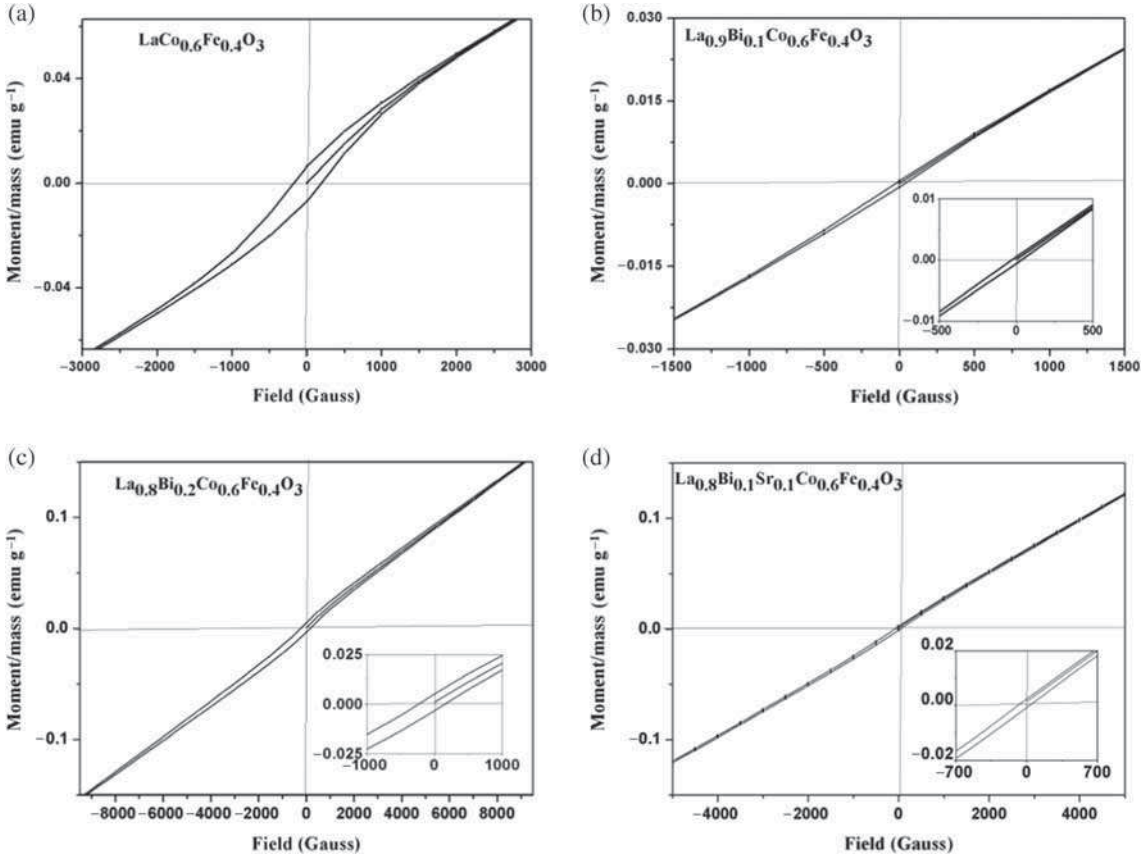

Figure 9. Vibrating sample magnetometer of samples (**a**) L0, (**b**) L1, (**c**) L2 and (**d**) L3 recorded at room temperature.

(Hc) = 183.78 G, remanance (Mr) = 6.69×10^{-3} emu g^{-1} and magnetic saturation (Ms) = 0.213 emu g^{-1}. It was already reported by Troyanchuk *et al* that the ferromagnetic nature of L0 is due to the percolation of Fe-rich clusters leading to the long-range ordering with fairly high coercive force. In all the compounds the magnetic ions present are cobalt and iron, which is in the mixed valance electron state as indicated by XPS studies. In these compounds the ferromagnetism arises as a result of exchange interaction between Co and Fe ions present in it. Although Fe makes the Co ions in $LaCo(Fe)O_3$ to low spin state which is diamagnetic, the strong interaction between the Fe ions caused by antisymmetric exchange interaction of the Dzyaloshinski-Moriya type spin-orbit coupling makes it ferromagnetic having large magnetic anisotropy [8,9]. It was obtained that, for L1 Hc = 31.73 G, Mr = 0.57×10^{-3} emu g^{-1}, Ms = 0.718 emu g^{-1}, for L2 Hc = 195 G, Mr = 4.21×10^{-3} emu g^{-1}, Ms = 0.193 emu g^{-1} and for L3, Hc = 58.27 G, Mr = 1.6×10^{-3} emu g^{-1} and Ms = 0.283 emu g^{-1}, respectively. Since Bi and Sr are diamagnetic, substitution of these elements leads to suppression of ferromagnetism. Even though the value of maximum magnetization increases with the incorporation of Bi or Sr, however none of these reaches saturation even at the maximum of the external fields provided [27].

4. Conclusions

Nanopowders of $La_{1-x}Bi_xCo_{0.6}Fe_{0.4}O_3$ ($x = 0$, 0.1, 0.2) and $La_{1-2x}Bi_xSr_xCo_{0.6}Fe_{0.4}O_3$ ($x = 0.1$) multinary perovskites were successfully synthesized by citrate sol–gel autocombustion method. All compounds have rhombhohedral crystal structure with $\bar{R}3c$ space group, Bi ($x = 0.2$) shows the presence of secondary peaks. From XRD data crystallite size, dislocation density and specific area were calculated. The lattice strain was obtained in the order of 0.001 for all compounds from Williamson's Hall linear fit plot. The grain size was found to be few hundred nanometres from SEM data. The EDAX result confirms the elemental composition. The core-level energy spectra of ions are deducted from XPS data. The oxidation state of La and Bi in all compounds was +3 without valence instability, Sr was found to be +2, Co and Fe have +3 oxidation states and the presence of satellite peaks. The substitution of Bi and Sr does not alter the oxidation state of La, Co and Fe ions in the perovskite configuration. The ratios of adsorbed oxygen to the lattice oxygen present in the samples were also found calculated and it confirms the presence of oxygen vacancies. From room temperature magnetic studies, it was observed that the replacement of La by Bi and Sr reduces the ferromagnetic property.

Acknowledgement

Megha U and Shijina K acknowledge the University Grant Commission, Government of India, for the BSR–RFSMS Fellowship.

References

[1] Joonghoe Dho and Hur N H 2006 *Solid State Commun.* **138** 152

[2] Yu J, Kamazawa K and Despina Louca 2010 *Phys. Rev. B* **82** 224101

[3] Yoshii K, Abe H and Nakamura A 2001 *Mater. Res. Bull.* **36** 1447

[4] Knizek K, Jirak Z, Hejtmanek J and Novak P 2006 *J. Phys. Condens. Matter* **18** 3285

[5] Senaris Rodriguez M A and Goodenough J B 1995 *J. Solid State Chem.* **118** 323

[6] Anderson P W and Hasegawa H 1955 *Phys. Rev.* **100** 675

[7] Klencsar Z, Nemeth Z, Kuzmann E, Homonnay Z, Vertes A, Hakl J, Vad K, Meszaros S, Simopoulos A, Devlin E, Kallias G, Greneche J M, Cziraki A and De S K 2008 *J. Magn. Magn. Mater.* **320** 651

[8] Troyanchuk I O, Karpinskii D V, Dobryanskii V M, Fedotova Yu A and Szymczak H 2005 *J. Exp. Theor. Phys.* **100** 1121

[9] Karpinskii D V, Troyanchuk I O, Barner K, Szymczak H and Tovar M 2005 *J. Phys.: Condens. Matter* **17** 7219

[10] Vulchev V, Vassilev L, Harizanova S, Khristov M, Zhecheva E and Stoyanova R 2012 *J. Phys. Chem. C* **116** 13507

[11] Bin F, Song C, Lv G, Song J, Gong C and Huang Q 2011 *Ind. Eng. Chem. Res.* **50** 6660

[12] Xiutao Ge, Yafei Liu and Xingqin Liu 2001 *Sens. Actuators B* **79** 171

[13] Royer S, Van Neste A, Davidson R, McIntyre S and Kaliaguine S 2004 *Ind. Eng. Chem. Res.* **43** 5670

[14] Megha U, Shijina K and Varghese G 2014 *Process. Appl. Ceramics* **8** 87

[15] Ravindran P, Vidya R, Kjekshus A, Fjellvag H and Eriksson O 2006 *Phys. Rev. B* **74** 224412

[16] Melo D S, Marinho E P, Soledade L B, Melo D A, Lima S G, Longo E, Garcia Santos I M and Souza A G 2008 *J. Mater. Sci.* **43** 551

[17] Liu X, Gao F and Tian C 2008 *Mater. Res. Bull.* **43** 693

[18] Kumar A, Verma A S and Bhardwaj S R 2008 *Open Appl. Phys. J.* **1** 11

[19] Rita John and Rajaram Rajakumari 2012 *Nano-Micro Lett.* **4** 65

[20] R W M Kwok available from: http://www.phys.cuhk.edu.hk/~surface/XPSPEAK

[21] Shirley D A 1972 *Phys. Rev. B* **5** 4709

[22] Vegh J 2006 *J. Electron Spectrosc. Rel. Phenom.* **151** 159

[23] Galenda A, Natile M M, Krishnan V, Bertagnolli H and Glisenti A 2007 *Chem. Mater.* **19** 2796

[24] Tie Li, Jianfeng Shen, Na Li and Mingxin Ye 2013 *J. Alloys Comp.* **548** 89

[25] Worayingyong A, Kangvansura P, Ausadasuk S and Praserthdam P 2008 *Colloids Surf. A: Physicochem. Eng. Asp.* **315** 217

[26] Natile M M, Fabio Poletto, Alessandro Galenda, Antonella Glisenti, Tiziano Montini, Loredana De Rogatis and Paolo Fornasiero 2008 *Chem. Mater.* **20** 2314

[27] Zhao Y D, Park J, Jung R-J, Noh H-J and Oh S-J 2004 *J. Magn. Magn. Mater.* **280** 404